12,11

Microstructure features of nanosized AsSb precipitates in LT-GaAsSb

©
L.A. Snigirev[1], A.V. Myasoedov[1], N.A. Bert[1], V.V. Preobrazhenskii[2], M.A. Putyato[2], B.R. Semyagin[2], V.V. Chaldyshev[1]

[1] Ioffe Institute,
St. Petersburg, Russia
[2] Rzhanov Institute of Semiconductor Physics, Siberian Branch, Russian Academy of Sciences,
Novosibirsk, Russia

E-mail: leonidsnigirev17@gmail.com

Received November 24, 2023
Revised November 24, 2023
Accepted November 24, 2023

The structural state of AsSb precipitates formed upon annealing of non-stoichometric $GaAs_{0.97}Sb_{0.03}$, epitaxial layer grown by molecular beam epitaxy on a GaAs (001) substrate at a temperature of 150°C, was investigated using transmission electron microscopy. New orientation relationships between AsSb precipitates with a rhombohedral lattice and the zincblende LT-GaAsSb matrix subjected to isothermal annealing at temperatures below 800°C for 15 minutes, were discovered: $\{\bar{1}012\}_p \parallel \{111\}_m$ and $\langle\bar{2}20\bar{1}\rangle_p \parallel \langle 1\bar{1}0\rangle_m$. These orientation relationships differ from those known for As precipitates $(0003)_p \parallel \{111\}_m$; $\langle\bar{1}2\bar{1}0\rangle_p \parallel \langle 1\bar{1}0\rangle_m$ and take place for particles with size less than ~ 10 nm. For particles smaller than ~ 7 nm, electron microscopy results allow to hypothesize a transition to the cubic phase $Pm\bar{3}m$.

Keywords: Non-stoichiometric GaAsSb, precipitation, transmission electron microscopy, orientation relationships.

DOI: 10.61011/PSS.2023.12.57698.263

1. Introduction

Gallium arsenide grown at low (150−350°C) temperature (LT-GaAs) by molecular-beam epitaxy (MBE) turns out to be highly non-stoichiometric due to the capture of excess arsenic in the growing crystal [1–3]. When annealing in the temperature range of 400−600°C, diffusion decomposition of the supersaturated solid solution of As in LT-GaAs occurs with the precipitation of excess arsenic into nanoscale crystalline particles (precipitates) [4,5]. As a result the material acquires a high resistivity ($\sim 10^8\,\Omega\cdot$cm), while keeping a short (< 1 ps) lifetime of charge carriers [6,7]. Such properties make it attractive for creating semiconductor photoconductive antennas for detecting and generating terahertz radiation [8,9], photodetectors and photomixers [10], and fast photoresistive switches [11].

Precipitation of As in LT-GaAs was studied in details, in particular, in the paper [12] it was found that the precipitates are spherical in shape and have an inherent α-As rhombohedral crystal lattice with space group $R\bar{3}m$, and their orientation relationships (OR) with LT-GaAs matrix in a hexagonal four index notation are defined as

$$(0003)_p \parallel \{\bar{1}1\bar{1}\}_m \quad \text{and} \quad \langle\bar{1}2\bar{1}0\rangle_p \parallel \langle 1\bar{1}0\rangle_m, \qquad (1)$$

where the subscripts p and m refer to the As precipitate and LT-GaAs matrix, respectively.

However, in LT-GaAs with delta-layers of GaSb [13] and solid solutions of LT-GaAsSb [14,15], along with particles of the rhombohedral phase with the above OR (1), precipitates were observed, whose microstructure and/or OR did not correspond to the configuration for α-As. When studying $LT\text{-}Al_{0.3}Ga_{0.7}As_{0.97}Sb_{0.03}$ it was established that in the precipitated particles of the second phase the Sb content greatly exceeds its concentration in the matrix [16,17], i.e. the particles are an alloy $As_{1-x}Sb_x$. AsSb has the same structure as arsenic and antimony with space group $R\bar{3}m$ [18], and $As_{0.5}Sb_{0.5}$, natural crystals of which are called stibarsen, is characterized by the presence of atomic ordering of GeTe type [19]. In terms of lattice constants, Sb differs significantly from arsenic, whose precipitates are semi-coherently incorporated into the sphalerite lattice of the LT-GaAs matrix. The lattice mismatch between AsSb and LT-GaAs and the corresponding increase in the elastic energy of the particle can affect its structural behavior in the matrix [20,21]. Additional interest in the microstructure of AsSb inclusions is caused by the detection in the optical spectra of $LT\text{-}Al_{0.3}Ga_{0.7}As_{0.97}Sb_{0.03}$ of signs of plasmon resonance due to the presence of an ensemble of nanosized particles and not observed in LT-GaAs [22,23]. The existence of plasmon resonance in the system of AsSb nanoparticles enriched with antimony and embedded in AlGaAs matrix is predicted by theoretical calculations performed for nanoinclusions with a rhombohedral atomic structure [24].

The goal of the paper was to determine the structural features of AsSb precipitates in $LT\text{-}GaAs_{0.97}Sb_{0.03}$ matrix using transmission electron microscopy (TEM).

2. Experimental procedure

Epitaxial layers of $LT\text{-}GaAs_{0.97}Sb_{0.03}$ were grown using the MBE method on GaAs substrate with a surface

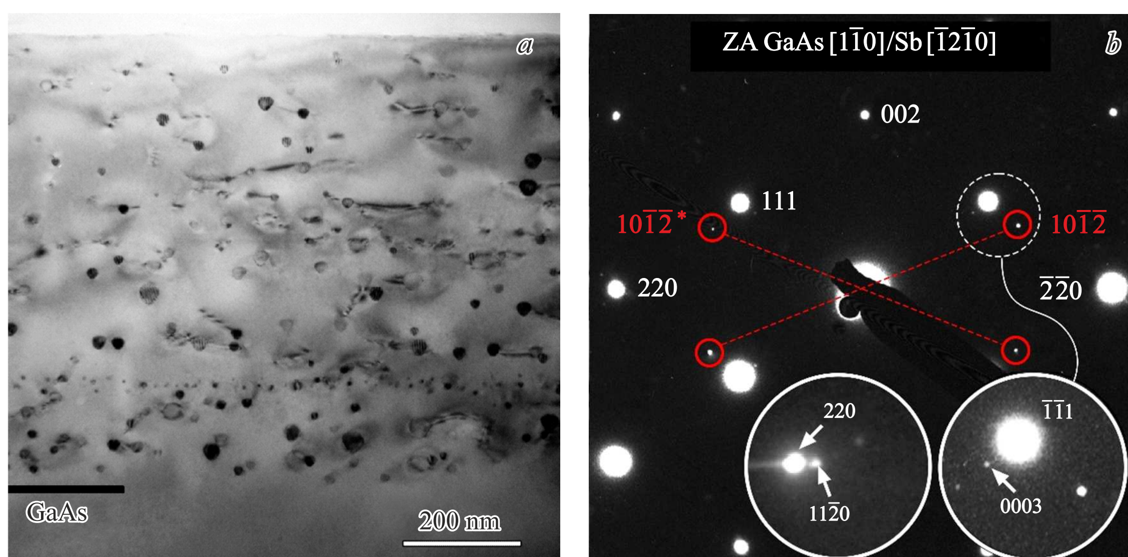

Figure 1. Cross-sectional bright-field TEM-image of the epitaxial layer of LT-$GaAs_{0.97}Sb_{0.03}$/GaAs in the zone axis $[1\bar{1}0]$ (*a*) and the corresponding electron diffraction pattern (*b*) after annealing at a temperature 800°C. Red circles indicate second phase reflexes. The asterisk indicates a pair of reflections from the second variant of particle arrangement due to the symmetry of the matrix. The inserts in the lower right part show enlarged fragments of the diffraction pattern in the vicinity of the matrix reflexes $\bar{1}\,\bar{1}1$ and 220.

orientation of $(001) \pm 0.5°$. Preliminary, GaAs buffer layer with a thickness of 200 nm was grown on the substrate at a temperature of 580°C. Then the temperature was reduced to 150°C, and LT-$GaAs_{0.97}Sb_{0.03}$ was deposited. At such low temperature the problem of epitaxial growth failure arises [25,26], which does not allow the growth of a relatively thick ($\sim 1\,\mu$m) layer. To prevent growth failure, the process was monitored by recording the reflection high-energy electron diffraction (RHEED) pattern. When signs of diffuse scattering associated with the surface roughening of the growing layer appeared, the process was stopped by shutting off the Ga flow, the temperature increased to 250°C and was maintained until the contribution of diffuse scattering disappeared in the RHEED pattern. After this, the temperature dropped again to 150°C, and growth resumed. To obtain a layer $1\,\mu$m thick, this technique was required twice. Upon growth completion of LT-$GaAs_{0.97}Sb_{0.03}$ layer, AlAs film 5 nm thick was deposited on its surface, performing the function of a diffusion barrier, and a GaAs film 5 nm thick was deposited for AlAs protection from oxidation. The resulting sample was divided into several parts, which were annealed in the growth chamber of the MBE installation under vapor backpressure conditions As_4 for 15 min at a temperature of 400, 500 or 600°C. Two parts, „folded face-to-face“, were subjected to rapid thermal annealing at 800°C in STE RTA100 unit (CJSC „NTO“, Russia) in nitrogen atmosphere.

Structural studies of the obtained samples were carried out by TEM using JEM-2100F microscope (JEOL, Japan) at an accelerating voltage of 200 kV and Phillips EM420 microscope at accelerating voltage of 100 kV. Samples for electron microscopy studies were prepared in two orientations — (001) plan-view and (110) cross section, by mechanical grinding-polishing and finishing ion milling. Fourier analysis of images obtained in high-resolution mode (HREM) was performed using the Digital Micrograph software package (Gatan, Inc. USA).

3. Experimental results

Figure 1, *a* shows an overview cross-sectional TEM-image of LT-$GaAs_{0.97}Sb_{0.03}$/GaAs epitaxial layer, annealed at temperature 800°C. In the image AsSb precipitates deposited as a result of annealing are shown in the form of spots of dark contrast, randomly distributed throughout the epitaxial layer. The high annealing temperature led to the generation of structural defects associated with the precipitated particles, creating a characteristic contrast in the image. The measured average particle size is 17 nm. Besides, in the lower region of the layer at a distance of about 190 nm from the boundary with GaAs buffer layer, a number of small inclusions is observed, apparently formed as a result of decorating the growth surface with particles of the residual atmosphere during an intermediate Growth Interruption [27]. A characteristic electron diffraction pattern (Figure 1, *b*) obtained along zone axis $[1\bar{1}0]$ from the same layer, together with the reflexes of LT-$GaAs_{0.97}Sb_{0.03}$ matrix contains extra-reflexes from the ensemble of particles of the second phase. Due to the small volume fraction of the second phase, the reflexes from particles have weak intensity. The resulting pattern contains four additional reflexes (marked with red circles), located near reflections 111 of the matrix and deviating from the corresponding axes $\langle 111 \rangle$ of the matrix by angle 13°. The interplanar spacing

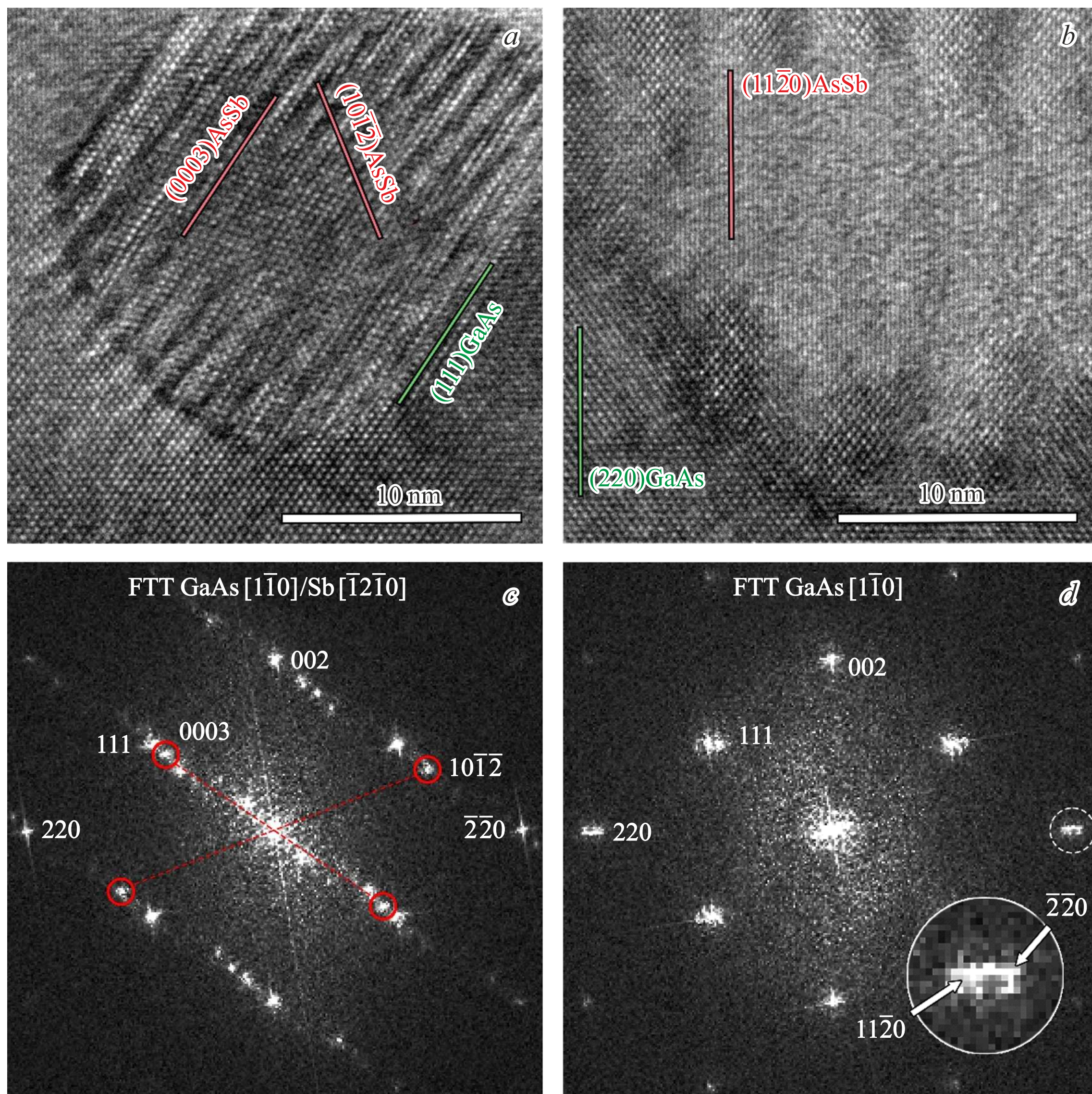

Figure 2. HREM-images of precipitates AsSb in LT-$GaAs_{0.97}Sb_{0.03}$, annealed at temperature 800°C (*a, b*) and corresponding to them patterns FFT (*c, d*). Insert: zoom in fragment of diffraction pattern in area of reflex $\bar{2}\bar{2}0$ of matrix, marked by dashed circle.

measured by the diffraction pattern for these additional reflexes $d = 3.04$ Å, and taking into account the fact that the particles are AsSb solution, the corresponding planes are indicated as $(10\bar{1}\bar{2})$ of the rhombohedral lattice. Near $\bar{1}\bar{1}1$ in the direction coinciding with the axis $[\bar{1}\bar{1}1]$ of the matrix, there is another weak reflex, more clearly presented in the insert in the lower right corner of Figure 1, *b*. The interplanar spacing for this reflex is measured as 3.76 Å and corresponds to the plane (0003) of the precipitate lattice. With a slight deviation from the zone axis $[1\bar{1}0]$ an additional reflex appears in the diffraction pattern near the matrix reflection 220, the reflex lies on the axis $[1\bar{1}0]$ of the matrix. It is shown in the insert in the lower central part of Figure 1, *b*. The corresponding interplanar spacing is $d = 2.10$ Å, and the planes are indicated as $(11\bar{2}0)$.

The location of the additional reflexes in Figure 1, *b* taking into account four variants of particle orientation due to the presence in the matrix of a an inversion axis of four-fold symmetry and changed interplanar spacings due to the presence of antimony in the particle, corresponds to precipitates of the rhombohedral phase, (0003) plane of which is parallel to one of the four planes {111} of the matrix. The location of the reflex $11\bar{2}0$ from precipitates on the matrix axis [110] specifies the second OR: $\langle 11\bar{2}0\rangle_p \parallel \langle 1\bar{1}0\rangle_m$. Such relationships are similar to the known ORs (1) for As precipitates of the rhombohedral phase in LT-GaAs [12].

Using the measured interplanar spacings and Vegard's law, the Sb content in precipitates can be estimated. Neglecting elastic deformations in the particle, which are obviously small due to the relaxation of misfit stresses with

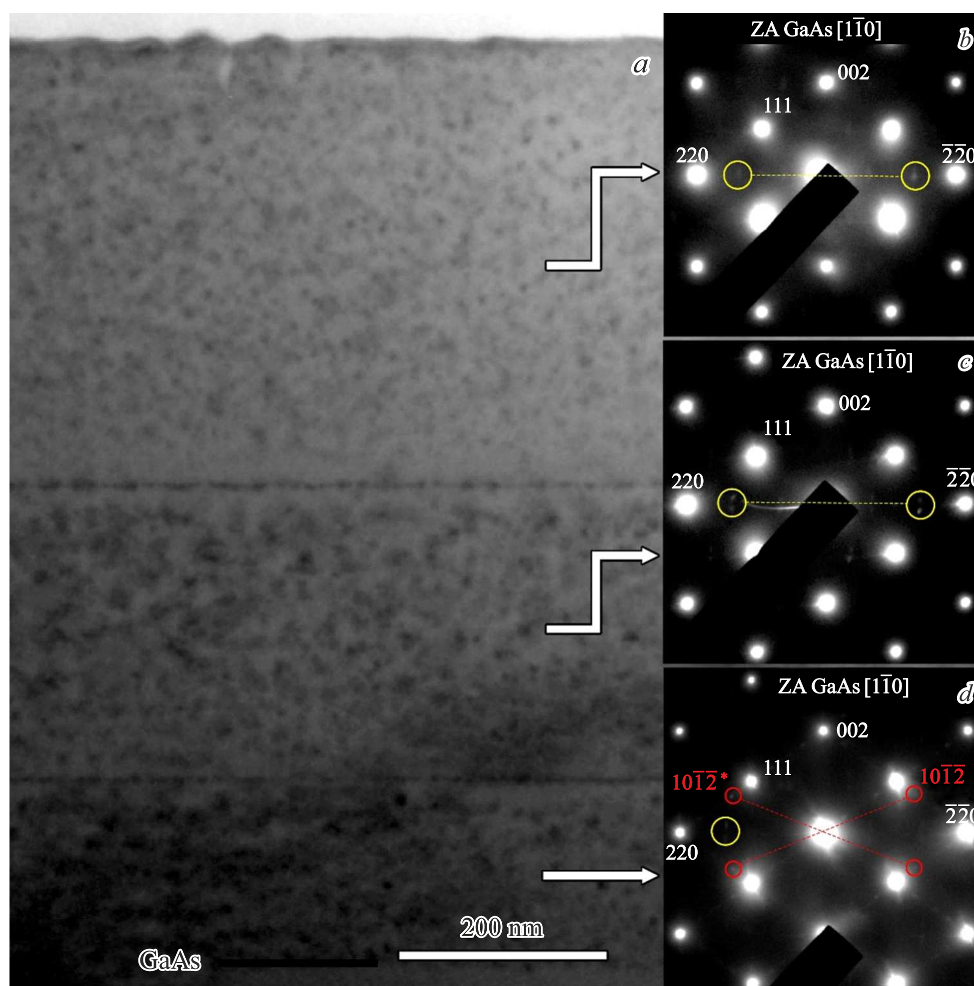

Figure 3. Bright-field TEM image of sample annealed at 400°C, in the active reflex 002 (*a*) and patterns of electron microdiffraction from different regions of LT-$GaAs_{0.97}Sb_{0.03}$ epitaxial layer. Yellow circles indicate atypical reflexes.

the generation of defects observed in Figure 1, *a*, the fraction of antimony turns out to be 0.8.

The data obtained from diffraction patterns on the microstructure and OS of deposited particles in LT-$GaAs_{0.97}Sb_{0.03}$ after annealing at 800°C are confirmed by the results of their studies in the HRTEM mode. Figure 2 shows examples of typical HRTEM images of precipitates and the corresponding Fourier images obtained by fast Fourier transform (FFT). Figure 2, *a* shows an AsSb particle observed in the zone axis $[\bar{1}2\bar{1}0]_p \parallel [1\bar{1}0]_m$. In the center of the particle image, the atomic planes in it are clearly visible.

The interplanar spacings measured from the image and FFT pattern correspond to (0003) and $\{10\bar{1}\bar{2}\}$. It can be seen that the FFT pattern for individual particle is quite consistent with the diffraction pattern from the ensemble of precipitates in Figure 1, *b*. Figure 2, *b* shows image of the particle rotated by 90° around the matrix axis [001] relative to the one shown in Figure 2, *a*. In the image of the particle and the FFT there are planes $(11\bar{2}0)$ parallel to the planes (220) of the matrix and close to them in interplanar spacings. This situation also corresponds to the diffraction pattern in Figure 1, *b*.

Lowering the annealing temperature to 600°C leads to a decrease in the average particle size to 9.8 nm, and along with the precipitates described above, individual particles with a different phase and/or other ORs are detected. With a further decrease in the annealing temperature to 500°C, the average particle size becomes 7.1 nm, and particles with nontrivial configuration are more common. After annealing at 400°C the fraction of such particles increases even more. Figure 3, *a* shows an overview image of LT-$GaAs_{0.97}Sb_{0.03}$ epitaxial layer subjected to post-growth annealing at 400°C.

The image shows two horizontal lines of dark contrast, containing small inclusions and resulting from a double growth interruption with low-temperature heating to 250°C. They divide the epitaxial layer into three regions. In the lower region of the layer, which was heated twice, the average particle size is 7.5 nm, in the middle region with single heating, 7.0 nm, and in the upper region, which was not subjected to intermediate heating, the average size decreases to 4.9 nm.

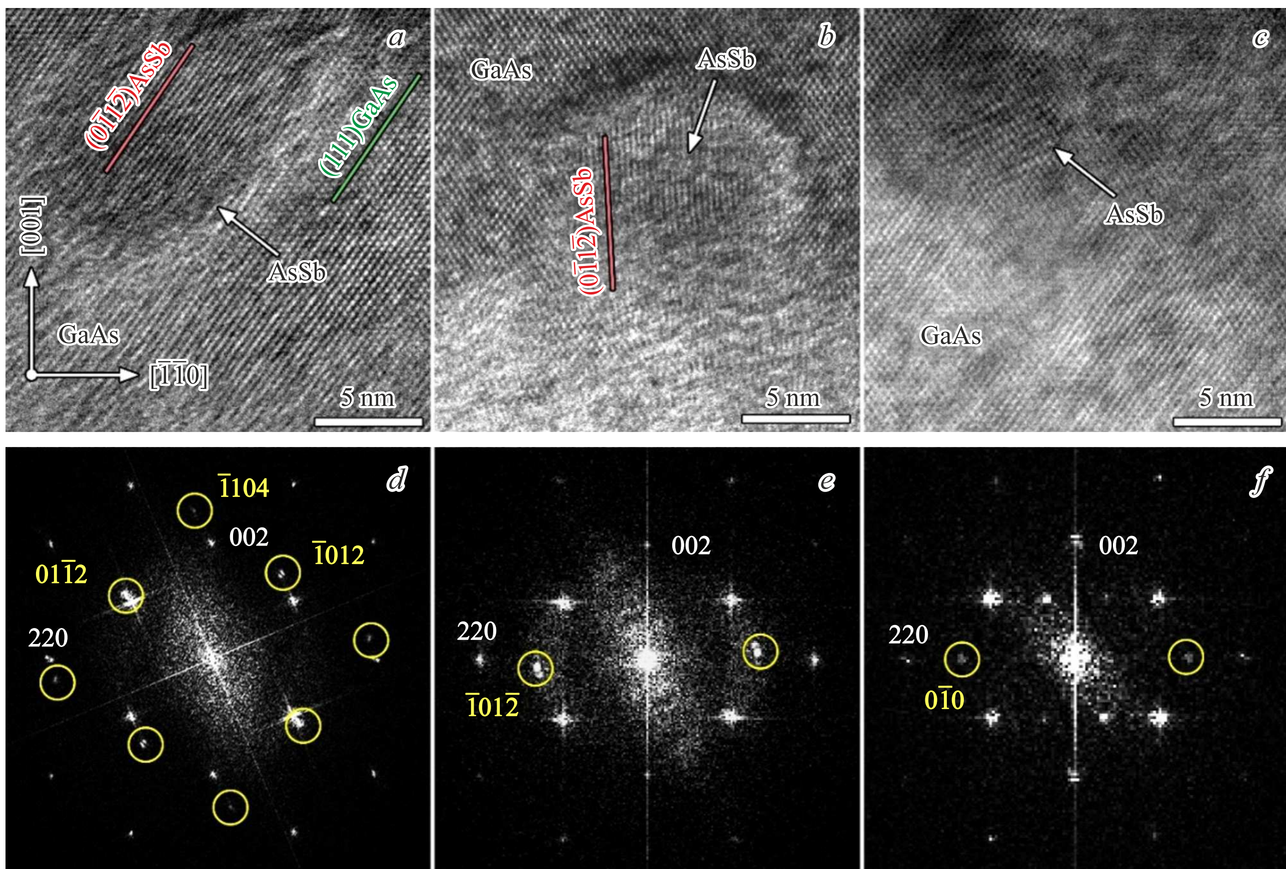

Figure 4. HRTEM images of AsSb precipitates in LT-$GaAs_{0.97}Sb_{0.03}$ annealed at temperature 400°C (*a, b, c*), and the corresponding to them FFT patterns (*d, e, f*). Yellow circles indicate reflexes from the second phase.

Typical diffraction patterns from each of the regions of the epitaxial layer of LT-$GaAs_{0.97}Sb_{0.03}$ are presented in Figure 3, *b, c* and *d*. The diffraction pattern from the lower region of the layer (Figure 3, *d*) there are reflexes inherent to rhombohedral phase with general OR (marked with red circles). At the same time, two weaker reflections are present, symmetrical with respect to the matrix direction [110] with a deviation from it by an angle 4° (marked with a yellow circle). The corresponding interplanar spacings are determined as 2.97 Å, which is close to the value for $\{10\bar{1}\bar{2}\}$. Only these reflexes appear in the diffraction pattern from the middle region (Figure 3, *c*). For the upper region with the smallest particle size, the same reflexes turn out to be located practically on the axis [110] of the matrix (Figure 3, *b*).

AsSb precipitates in samples annealed at temperatures 600°C and below were also studied in the HRTEM mode. Characteristic images of particles with unusual configuration in sample annealed at 400°C and the corresponding Fourier transform are presented in Figure 4.

As you can see, the FFT patterns do not correspond to the usual ORs, but the position of the reflexes in Figure 4, *e, f* is quite consistent with the SAED patterns (Figure 3, *b, c*). The FFT pattern in Figure 4, *d* also does not coincide with the usual ORs, and is obviously obtained from the particle in another projection, corresponding to its rotation by 90° around the axis of symmetry [001] of matrix. The indication of reflections in the FFT patterns of Figure 4, *d, e* was carried out using the measured interplanar spacings and angles in the representation of the rhombohedral system. The position of the reflexes in Figure 4, *f* exactly on the matrix axis [110] allows us to consider the structure as cubic, which is discussed below.

4. Discussion

Thus, the above experimental results indicate that in the studied samples with post-growth annealing temperature 400°C, along with precipitates of the rhombohedral phase and ORs determined in [12], the precipitates with different ORs or with a different crystal lattice are formed. The fraction of such precipitates decreases with increasing annealing temperature and a corresponding increase in their average size until complete disappearance after annealing at 800°C, when the average particle size reaches 17 nm. The interpretation of the obtained data for small precipitates was carried out using modeling of the diffraction patterns under the condition that one of the planes of the family $\{10\bar{1}\bar{2}\}_p$

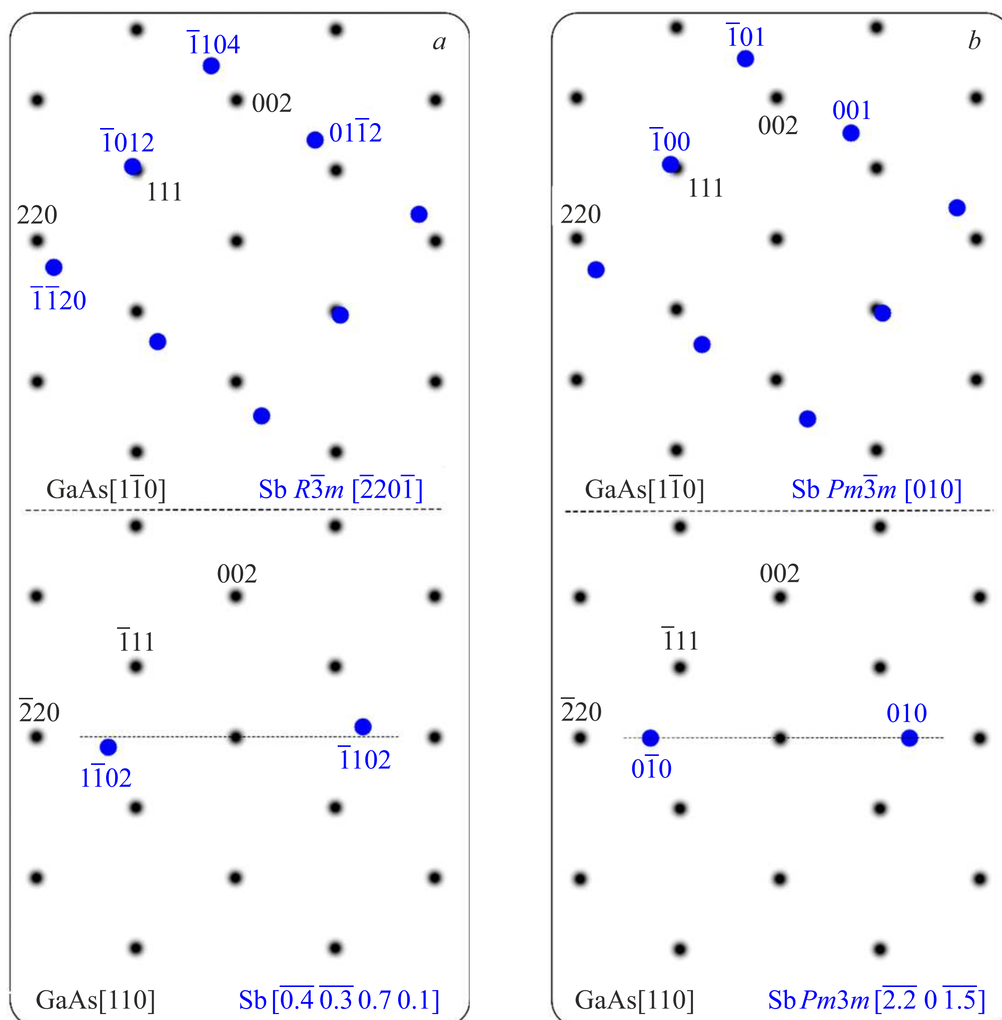

Figure 5. Simulated diffraction patterns of AsSb particles in two mutually perpendicular zone axes of LT-GaAsSb matrix for the rhombohedral (*a*) and simple cubic (*b*) phase.

of the AsSb rhombohedral lattice is parallel to the (111) GaAsSb plane. The variant that satisfies the experimental data is shown in Figure 5, *a* for two mutually perpendicular zone axes of the matrix.

According to the simulated pattern, reflexes $\bar{1}10\bar{2}$ and $1\bar{1}02$ from the precipitate observed in the zone axis [110] of the matrix (lower part of Figure 5, *a*), are located at angle 3° relative to the matrix direction $[1\bar{1}0]_m$. This situation occurs in the diffraction patterns in Figure 3, *c, d* and the FFT pattern in Figure 4, *e*. But in Figure 3, *a* and 4, *f* these reflexes turn out to lie directly on the matrix axis $[1\bar{1}0]_m$. This may be due to some distortion of the rhombohedral lattice. On the other hand, antimony outside normal conditions can crystallize into a simple cubic lattice [28–31], with $a \approx 3$ Å. The simulated diffraction pattern for simple lattice $As_{0.2}Sb_{0.8}$ provided that the $(\bar{1}00)_p$ plane is parallel to the matrix plane $(111)_m$ is shown in Figure 5. *b*. The diffraction pattern obtained in the experiment for the ensemble of particles with average size of 4.9 nm (Figure 3, *b*) and the FFT pattern for small (7 nm) particle (Figure 4, *f*) have exactly this form.

The combination of experimental data and calculated results shows that for precipitates $As_{0.2}Sb_{0.8}$ with average size ~ 10 nm and less, having a rhombohedral lattice, the following ORs are predominantly satisfied:

$$\{\bar{1}012\}_p \parallel \{111\}_m \quad \text{and} \quad \langle\bar{2}20\bar{1}\rangle_p \parallel \langle 1\bar{1}0\rangle_m. \qquad (2)$$

The data obtained do not allow us to unambiguously determine whether the crystal lattice of precipitates $As_{0.2}Sb_{0.8}$ with size less than 7 nm is rhombohedral or cubic. If the lattice is cubic, then for OR with matrix LT-$GaAs_{0.97}Sb_{0.03}$ the following relations are satisfied

$$\{\bar{1}00\}_p \parallel \{111\}_m \quad \text{and} \quad \langle 0\bar{1}0\rangle_p \parallel \langle 1\bar{1}0\rangle_m. \qquad (3)$$

5. Conclusion

TEM method was used to study the structural state of AsSb precipitates formed as a result of annealing

of epitaxial layer of non-stoichiometric LT-$GaAs_{0.97}Sb_{0.03}$ grown by MBE on GaAs(001) substrate at temperature 150°C. It is established that precipitates with the average size greater than ~ 7 nm have conventional rhombohedral lattice with the space group $R\bar{3}m$, inherent to As and Sb under normal conditions. For precipitates with the average size less than ~ 10 nm new orientation relationships with LT-GaAsSb matrix were discovered: $\{\bar{1}012\}_p \parallel \{111\}_m$ and $\langle\bar{2}20\bar{1}\rangle_p \parallel \langle 1\bar{1}0\rangle_m$. TEM results for particles with average size less than ~ 7 nm give grounds to assume the presence of the cubic phase.

Funding

The study was supported by a grant from the Russian Science Foundation No. 22-22-20105 (https://rscf.ru/project/22-22-20105/) and a grant from the St. Petersburg Science Foundation in accordance with the agreement dated April 14, 2022 No. 25/2022.

Conflict of interest

The authors declare that they have no conflict of interest.

References

[1] M.R. Melloch, J.M. Woodall, E.S. Harmon, N. Otsuka, F.H. Pollak, D.D. Nolte, R.M. Feenstra, M.A. Lutz. Annu. Rev. Mater. Sci. **25**, *1*, 547 (1995). doi: 10.1146/annurev.ms.25.080195.002555.

[2] L.G. Lavrent'eva, M.D. Vilisova, V.V. Preobrazhenskii, V.V. Chaldyshev. Russ. Phys. J. **45**, *8*, 735 (2002). doi: 10.1023/A:1021965211576/METRICS.

[3] X. Liu, A. Prasad, J. Nishio, E.R. Weber, Z. Liliental-Weber, W. Walukiewicz. Appl. Phys. Lett. **67**, *2*, 279 (1995). doi: 10.1063/1.114782.

[4] M.R. Melloch, N. Otsuka, J.M. Woodall, A.C. Warren, J.L. Freeouf. Appl. Phys. Lett. **57**, *15*, 1531 (1990). doi: 10.1063/1.103343.

[5] N.A. Bert, A.I. Weinger, M.D. Vilisova, S.I. Goloshchapov, I.V. Ivonin, S.V. Kozyrev, A.E. Kunitsyn, L.G. Lavrentieva, D.I. Lubyshev, V.V. Preobrazhensky, B.R. Semyagin, V.V. Tretyakov, V.V. Chaldyshev. FTT **35**, *10*, 2609 (1993). (in Russian).

[6] I.S. Gregory, C. Baker, W.R. Tribe, M.J. Evans, H.E. Beere, E.H. Linfield, A.G. Davies, M. Missous. Appl. Phys. Lett. **83**, *20*, 4199 (2003). doi: 10.1063/1.1628389.

[7] A.A. Pastor, U.V. Prokhorova, P.Y. Serdobintsev, V.V. Chaldyshev, M.A. Yagovkina. Semiconductors **47**, *8*, 1137 (2013). doi: 10.1134/S1063782613080150/METRICS.

[8] H. Tanoto, J.H. Teng, Q.Y. Wu, M. Sun, Z.N. Chen, S.A. Maier, B. Wang, C.C. Chum, G.Y. Si, A.J. Danner, S.J. Chua. Nat. Photonics **6**, *2*, 121 (2012). doi: 10.1038/nphoton.2011.322.

[9] R. Jiang, S. Cheng, Q. Li, Q. Wang, Y. Xin. Laser Phys. **31**, *3*, 036203, (2021). doi: 10.1088/1555-6611/ABD935.

[10] M. Currie. In: Photodetectors: Materials, Devices and Applications. Woodhead Publishing (2016). P. 121–155. doi: 10.1016/B978-1-78242-445-1.00005-1.

[11] C. Tannoury, M. Billet, C. Coinon, J.F. Lampin, E. Peytavit. Electron. Lett. **56**, *17*, 897 (2020). doi: 10.1049/EL.2020.1116.

[12] A. Claverie, Z. Liliental-Weber. Phil. Mag. A Phys. Condens. Matter, Struct. Defects Mech. Prop. **65**, *4*, 981 (1992). doi: 10.1080/01418619208205601.

[13] N.A. Bert, V.V. Chaldyshev, A.A. Suvorova, V.V. Preobrazhenskii, M.A. Putyato, B.R. Semyagin, P. Werner. Appl. Phys. Lett. **74**, *11*, 1588 (1999). doi: 10.1063/1.123625.

[14] J. Sigmund, C. Sydlo, H.L. Hartnagel, N. Benker, H. Fuess, F. Rutz, T. Kleine-Ostmann, M. Koch. Appl. Phys. Lett. **87**, *25*, 1 (2005). doi: 10.1063/1.2149977.

[15] J. Sigmund, D. Pavlidis, H.L. Hartnagel, N. Benker, H. Fuess. J. Vac. Sci. Technol. B **24**, *3*, 1556 (2006). doi: 10.1116/1.2190677.

[16] N.A. Bert, V.V. Chaldyshev, N.A. Cherkashin, V.N. Nevedomskiy, V.V. Preobrazhenskii, M.A. Putyato, B.R. Semyagin, V.I. Ushanov, M.A. Yagovkina. J. Appl. Phys. **125**, 14 (2019). doi: 10.1063/1.5048076.

[17] N. Bert, V. Ushanov, L. Snigirev, D. Kirilenko, V. Ulin, M. Yagovkina, V. Preobrazhenskii, M. Putyato, B. Semyagin, I. Kasatkin, V. Chaldyshev. Mater. **15**, *21*, 7597 (2022). doi: 10.3390/MA15217597.

[18] Handbook of Mineralogy / Eds John W. Anthony, Richard A. Bideaux, Kenneth W. Bladh. Mineralogical Society of America, Chantilly, VA 20151-1110, USA.

[19] D.P. Shoemaker, T.C. Chasapis, D. Do, M.C. Francisco, D. Young Chung, S.D. Mahanti, A. Llobet, M.G. Kanatzidis. Phys. Rev. B **87**, 94201 (2013). doi: 10.1103/PhysRevB.87.094201.

[20] V.V. Chaldyshev, N.A. Bert, A.E. Romanov, A.A. Suvorova, A.L. Kolesnikova, V.V. Preobrazhenskii, M.A. Putyato, B.R. Semyagin, P. Werner, N.D. Zakharov, A. Claverie. Appl. Phys. Lett. **80**, *3*, 377 (2002). doi: 10.1063/1.1426691.

[21] V.V. Chaldyshev, A.L. Kolesnikova, N.A. Bert, A.E. Romanov. J. Appl. Phys. **97**, 2 (2005). doi: 10.1063/1.1833581/930326.

[22] V.I. Ushanov, V.V. Chaldyshev, N.A. Bert, V.N. Nevedomsky, N.D. Il'inskaya, N.M. Lebedeva, V.V. Preobrazhenskii, M.A. Putyato, B.R. Semyagin. Semiconductors **49**, *12*, 1587 (2015). doi: 10.1134/S1063782615120234/METRICS.

[23] L.A. Snigirev, V.I. Ushanov, A.A. Ivanov, N.A. Bert, D.A. Kirilenko, M.A. Yagovkina, V.V. Preobrazhensky, M.A. Putyato, B.R. Semyagin, I.A. Kasatkin, V.V. Chaldyshev. FTP **57**, *1*, 71 (2023). doi: 10.21883/ftp.2023.01.54933.4545. (in Russian).

[24] V.M. Silkin, S.V. Eremeev, V.I. Ushanov, V.V. Chaldyshev. Nanomater. **13**, *8*, 1355 (2023). doi: 10.3390/NANO13081355.

[25] D.J. Eaglesham, L.N. Pfeiffer, K.W. West, D.R. Dykaar. Appl. Phys. Lett. **58**, *1*, 65 (1991). doi: 10.1063/1.104446.

[26] Z. Liliental-Weber, W. Swider, K.M. Yu, J. Kortright, F.W. Smith, A.R. Calawa. Appl. Phys. Lett. **58**, *19*, 2153 (1991). doi: 10.1063/1.104990.

[27] L.A. Snigirev, N.A. Bert, V.V. Preobrazhensky, M.A. Putyato, B.R. Semyagin, V.V. Chaldyshev. FTP **57**, *6*, 507 (2023). (in Russian).

[28] D. Akhtar, V.D. Vankar, T.C. Goel, K.L. Chopra. J. Mater. Sci. **14**, *4*, 988 (1979). doi: 10.1007/BF00550732/METRICS.

[29] X.S. Wang, S.S. Kushvaha, Z. Yan, W. Xiao. Appl. Phys. Lett. **88**, *23*, 233105 (2006). doi: 10.1063/1.2208374.
[30] T. Gupta, K. Elibol, S. Hummel, M. Stöger-Pollach, C. Mangler, G. Habler, J.C. Meyer, D. Eder, B.C. Bayer. npj 2D Mater. Appl. **5**, *1*, 1 (2021). doi: 10.1038/s41699-021-00230-3.
[31] A.L. Coleman, M.G. Gorman, R. Briggs, R.S. McWilliams, D. McGonegle, C.A. Bolme, A.E. Gleason, D.E. Fratanduono, R.F. Smith, E. Galtier, H.J. Lee, B. Nagler, E. Granados, G.W. Collins, J.H. Eggert, J.S. Wark, M.I. McMahon. Phys. Rev. Lett. **122**, 25 (2019).
doi: 10.1103/PhysRevLett.122.255704.

Translated by I.Mazurov